| | |
|---|---|
| Title | Nanoscale electronic structure of the layered nitride superconductors α-KxTiNCl and β-HfNCly observed by scanning tunneling microscopy and spectroscopy |
| Auther(s) | Sugimoto, Akira; Shohara, Kazuhiro; Ekino, Toshikazu; Zheng, Zhanfeng; Yamanaka, Shoji |
| Citation | Physical Review B , 85 (14) : 144517 |
| Issue Date | 2012 |
| DOI | 10.1103/PhysRevB.85.144517 |
| Self DOI | |
| URL | http://ir.lib.hiroshima-u.ac.jp/00033925 |
| Right | (c) 2012 American Physical Society |
| Relation | |

# Nanoscale electronic structure of the layered nitride superconductors $\alpha$-$K_xTiNCl$ and $\beta$-$HfNCl_y$ observed by scanning tunneling microscopy and spectroscopy

Akira Sugimoto,[1] Kazuhiro Shohara,[1] Toshikazu Ekino,[1] Zhanfeng Zheng,[2] and Shoji Yamanaka[2]
[1]*Graduate School of Integrated Arts and Sciences, Hiroshima University, Higashi-Hiroshima 739-8521, Japan*
[2]*Graduate School of Engineering, Hiroshima University, Higashi-Hiroshima 739-8527, Japan*
(Received 13 May 2011; revised manuscript received 24 February 2012; published 17 April 2012)

Scanning tunneling microscopy and spectroscopy (STM-STS) measurements have been carried out on the $\alpha$ (FeOCl)–type $K_xTiNCl$ ($x \sim 0.5$, $T_c = 16$ K) and $\beta$ (SmSI)–type $HfNCl_y$ ($y \sim 0.7$, $T_c = 24$ K) layered nitride superconductors. The STM images at 5 K showed clear atomic arrangements for both the compounds, namely, the rectangular lattice on $\alpha$-$K_xTiNCl$ and the triangular lattice on $\beta$-$HfNCl_y$. The tunneling spectra in the superconducting states at low temperatures demonstrate qualitatively different features between these superconductors. For $\alpha$-$K_xTiNCl$, the spatial distributions of the density of states and the superconducting gap structures are very inhomogeneous, while those on $\beta$-$HfNCl_y$ are found to be almost homogeneous. The nanoscale electronic features between these compounds correlate with the different lattice structures of the $M$ (=Ti or Hf) N conducting layers, which are caused by the lattice symmetry difference itself or induced by the difference in the local doping distributions in these chemically reactive compounds. The averaged gap magnitudes in the superconducting states, $\bar{\Delta} \simeq 10.2$ meV and 7.5 meV for $\alpha$-$K_xTiNCl$ and $\beta$-$HfNCl_y$, corresponding to the gap ratios $2\bar{\Delta}/k_BT_c \simeq 15$ and 7.2, respectively, indicate the unusually strong coupling effects of the superconductivity.

DOI: 10.1103/PhysRevB.85.144517 PACS number(s): 74.50.+r, 68.37.Ef, 74.70.−b, 74.81.−g

## I. INTRODUCTION

During the past decades, several kinds of superconductors with relatively higher critical temperatures ($T_c$), such as layered nitirides,[1] metal diborides,[2] and iron pnictides,[3] have been newly discovered. Almost all of them, including the cuprate superconductors, commonly have the two-dimensional (2D) layer structures. Among them, the layered nitride superconductors ($MNX$, $M$ = Zr, Hf, Ti; $X$ = Cl, Br, I) with the maximum $T_c$ of 25.5 K ($M$ = Hf, $X$ = Cl) were discovered in 1998 by Yamanaka *et.al.*[1] The electronic states of these materials can be systematically controlled by tuning both carrier-doping level and the layer separation by the atomic intercalation. Therefore, it should be very suitable for the systematic investigations to compare mutually the necessary conditions of the occurrence of the superconductivity.

There are now two types of the layered nitride compounds; one is the $\alpha$ (FeOCl)–type structure with the 2D metal-nitrogen ($M$N) layer of rectangular lattice [shown in Fig. 1(a)], and the other is the $\beta$ (SmSI)–type one with the 2D $M$N layer of honeycomb lattice [shown in Fig. 1(b)]. Therefore, these layered nitride superconductors are the rare kinds of materials that have different lattice structures in the same compound family. The $\alpha$-type and the $\beta$-type ones can be comparable to the cuprate and magnesium diboride superconductors because the former compounds have the 2D-conductive rectangular lattice and the latter have the honeycomb lattice. In the case of $\beta$-type superconductors, many theoretical and experimental studies have been done, and recent studies showed that the compounds exhibit unconventional behaviors, such as the small isotope effect (∼0.07, Refs. 4 and 5) and the quite-low electronic specific-heat coefficient (∼1 mJ/mol $K^2$, Ref. 4). Our previous experiments of break-junction (BJ) tunnel spectroscopy showed relatively large gap $\Delta$ (the gap ratio is $2\Delta/k_BT_c = 5 \sim 6$)[6–8] with a BCS-like density of states. The specific-heat measurement of $\beta$-type ZrNCl also showed $2\Delta/k_BT_c \sim 5$ assuming the anisotropic $s$-wave gap.[9] These results suggest that they possess weak electron-phonon interaction and low carrier density but exhibit the strong-coupling superconductivity. In contrast to the $\beta$-type superconductor, the $\alpha$-type one has not been well investigated because it is difficult to synthesize and extremely reactive in air. Recently, the $\alpha$-type $K_xTiNCl$ superconductor was successfully synthesized with $T_c \sim 16$ K.[10] This would enable us to compare the superconductivity of different types of the conducting lattice network.

To clarify the properties of these two types of layered nitride superconductors, the investigations of the spatial variation of the electronic properties with atomic length scale must be very important. Among such experiments, the scanning tunneling microscopy-spectroscopy (STM-STS) method provides the most powerful tool to observe directly the local density of states (LDOS) with atomic resolution in real space. In fact, inhomogeneous electronic properties have been clarified in cuprate superconductors by the STS method, which gave unique and important contributions to understand the high-$T_c$ superconductivity.[11–13] Especially in the case of layered nitride superconductors, it is very interesting to investigate whether such inhomogeneous LDOS exists in compounds that have layered structures with different lattice symmetries of $\alpha$ (rectangular)– and $\beta$ (honeycomb)–type structures. Furthermore, we hope to understand further the mechanisms of superconductivity by comparing this material family with abovementioned cuprate and other recently discovered superconductors.

In this paper, we show the first observation of the atomic arrangements and spatial variation of tunnel spectra by the STM-STS technique on different types of $\alpha$- and $\beta$-layered nitride superconductors. The different atomic lattice structures of $\alpha$ and $\beta$ types are directly visualized from the STM images. From the measurements of the tunneling spectra and the gap distributions in these superconductors, significant differences are found between the two types of superconductors.

 

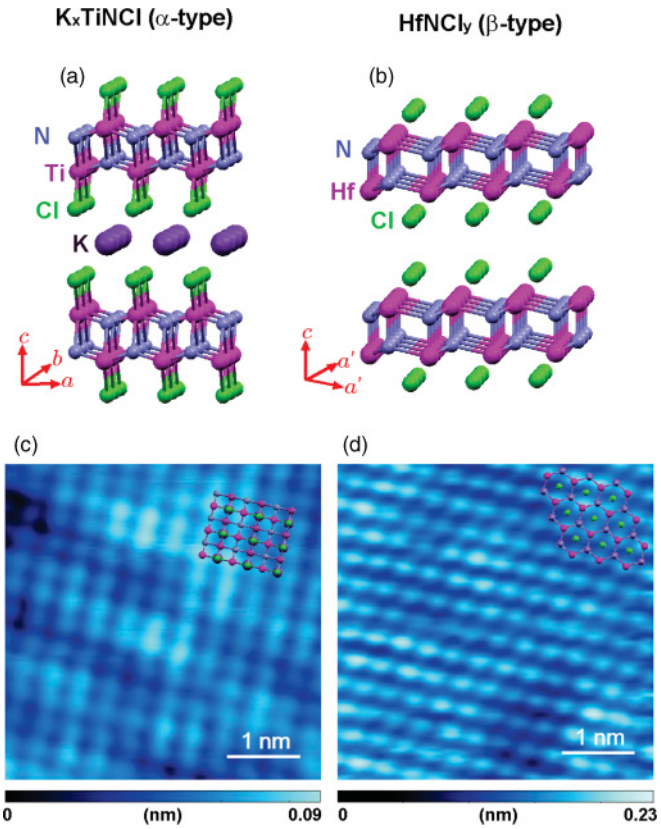


FIG. 1. (Color online) Schematic lattice structure of $\alpha$-$K_x$TiNCl (a) and STM image (c) ($I_t = 0.1$ nA, $V_{\text{sample}} = 0.1$ V). Schematic lattice structure of $\beta$-$HfNCl_y$ (b) and its STM image (d) ($I_t = 0.1$ nA, $V_{\text{sample}} = 0.1$ V). Schematic $ab(aa')$-plane lattice structures of each compound are superposed in panels (c) and (d).

## II. EXPERIMENTAL

The polycrystalline samples of $\alpha$-type $K_x$TiNCl ($x \sim 0.5$, $T_c \sim 16$ K) were prepared by reacting powder $\alpha$-TiNCl with metal azides $KN_3$ (potassium intercalation). On the other hand, the $\beta$-type $HfNCl_y$ samples ($y \sim 0.7$, $T_c \sim 24$ K) were prepared by reacting with alkali metal (potassium) formed by the thermal decomposition of azides $KN_3$ (chlorine deintercalation). The details of the fabrication of these samples have been already reported.[10,14] Since these samples were very reactive in air humidity, they were mounted on the STM sample holders in a pure Ar-filled grove box. The samples were then sealed in a container and carefully transferred to the ultrahigh vacuum (UHV) chamber ($P \sim 10^{-8}$ Pa) of the STM apparatus and cleaved at 77 K. The STM equipment used in this experiment is a commercially based system (Omicron LT-STM) with some modifications.[15,16] The STM-STS observations were carried out at the temperature of 4.9 K in UHV atmosphere of $\sim 10^{-8}$ Pa. Since the size of the single-crystal domain facet is about several tens of micrometers, it is enough to carry out the scanning operation by STM-STS. The STM topographies were measured by a constant-current mode. The $dI/dV$ curves were obtained by numerical differentiation of the measured $I - V$ characteristics with the spatial interval of $\sim$0.08 nm ($K_x$TiNCl) and $\sim$0.15 nm ($HfNCl_y$).

## III. RESULTS AND DISCUSSION

Figures 1(c) and 1(d) show STM images on the UHV-cleaved $K_x$TiNCl and $HfNCl_y$ surfaces, respectively, at 4.9 K. Since these compounds possess the layered structures, the cleavage surface is always the $ab$ ($aa'$) plane of the crystal. For $K_x$TiNCl, the rectangular atomic lattice distribution is clearly visible in the STM image, while the triangular distribution is obvious in the image of $HfNCl_y$. Therefore, we can easily confirm the difference between the network structures of $K_x$TiNCl and $HfNCl_y$ by STM topographies. From the fast-Fourier transform (FFT) analysis of the STM images, the periods of atomic corrugations on $K_x$TiNCl and $HfNCl_y$ are $|\vec{a}| = 0.41$ nm, $|\vec{b}| = 0.33$ nm, and $|\vec{a'}| = 0.36$ nm. These periods correspond to those observed by x-ray measurements ($|\vec{a}| = 0.406$ nm, $|\vec{b}| = 0.329$ nm for $K_x$TiNCl,[10] $|\vec{a'}| = 0.357$ nm for $HfNCl_y$[14]), thereby indicating that both the observed surfaces are $ab$ ($aa'$) plane of the single-crystal domain within the scanning area. Since the intervals of the atomic lattice separation correspond to the unit cell, a specific kind of atom is visible as the bright spots in the STM images. It is considered that some other kinds of atoms are invisible and/or they are observed as dark spots within the present measurement conditions. In our observed topographies of $HfNCl_y$ with the various bias voltages ($|V| < 0.5$ V), only one kind of lattice feature such as Fig. 1(d) was stably obtained. As shown in the schematic crystal structure of $ab$ ($aa'$) plane superposed on the STM images, all kinds of atoms (K, Ti or Hf, N, Cl) have the same interval distances at topmost or second-to-the-top surfaces. On the basis of the total amount of intercalated potassium (50% per unit cell) in $K_x$TiNCl and deintercalated chlorine (30% per unit cell) in $HfNCl_y$, the bright atomic spots do not exactly correspond to the occupied potassium atoms or deintercalated chlorine sites. Since the conducting layer of these compounds consists of the metal-nitride double layer, it is reasonable to believe that the observed structure is the network of the Ti-N or Hf-N layer.

For further understanding the surface properties, the bias voltage dependence of STM images has been measured, especially in $K_x$TiNCl. Figure 2 shows the STM images of the $K_x$TiNCl compound with the various bias voltages from $-0.2$ V to 0.3 V. By comparing the STM images, the positive-bias STM images [Figs. 2(a) and 2(b)] show clearer lattice structures than the negative-bias one [Fig. 2(c) and 2(d)]. The negative-bias images show a one-dimensional (1D) streak-like pattern in contrast to the spot-like pattern for the positive biases, which are indicated by the dashed lines in Figs. 2(c) and 2(d). According to the band calculations of TiNCl,[10] the filled state (negative-bias side) consists of N $2p$ and Ti $3d$ bands, while the empty state (positive-bias side) dominates the Ti $3d$ band. Then, STM can detect the convolution of atomic lattice structures and the N $2p$–Ti $3d$ hybrid band only in the negative bias. Within this condition, the STM images of the negative bias do not resolve atoms in the $b$-axis direction, because the $b$-axis length is shorter than the $a$-axis one; they show the 1D streaky pattern along the $b$ axis. Another important feature is that all of the STM images exhibit the inhomogeneous background pattern as surrounded by the dashed lines in Fig. 2(b). The enhanced bright areas occupy about $\simeq 0.55 \pm 0.10$ of whole the STM observed area, which

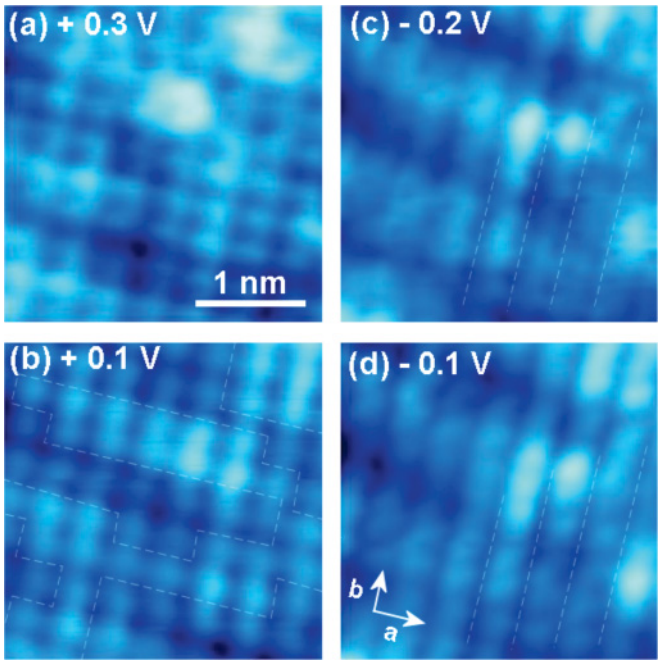


FIG. 2. (Color online) Bias dependence of STM image on $\alpha$-$K_x$TiNCl ($I_t = 0.1$ nA). Panels (a) and (b) are in the positive sample bias (0.3 V, 0.1 V), and panels (c) and (d) are in the negative sample bias (−0.2 V, −0.1 V).

is comparable to the nominal ratio of potassium intercalation ($x \sim 0.5$). Therefore, it is considered that these contrasts may be related to the intercalated atoms and/or doped carriers. The details of the STM topographies have been already discussed elsewhere.[17]

In order to clarify the surface electronic states and superconducting properties, it is necessary to inspect the atomic-scale LDOS and gap distributions. It is well known that the magnitude of $dI/dV$ is proportional to the LDOS; hence, the precise spatial distributions of LDOS are able to be obtained by many-point $dI/dV$ measurements. The 64 × 64 points of $dI/dV$ measurements were carried out, and then the $dI/dV$ maps of each bias voltage $V$ were derived from the magnitude of conductance of the corresponding bias voltage $[dI/dV(V)]$.

Figures 3(a)–3(j) show the $dI/dV$ maps with various sample bias voltages (for energy levels, see the figure captions) on $K_x$TiNCl derived from the $dI/dV$ spectra. The color scales of these maps are common (bottom of the figures): As the magnitude of the bias level is reduced, the contrast of the color changes darker. Clearly, almost all maps show the spatially inhomogeneous distributions of electronic states. Furthermore, these distributions largely depend on the bias voltages. For example, the distribution patterns are different between the bias polarities, especially around $|V| = 15$ mV. In the $dI/dV$ map of $V \sim -15$ mV [Fig. 3(c)], the brighter area is clearly observed near the center (indicated by arrow), while in that of $V \sim 15$ mV [Fig. 3(h)], the bright areas of Fig. 3(c) turn to the dark area. Figures 3(k)–3(o) show the $dI/dV$ maps on $HfNCl_y$ with various sample bias voltages. Obviously, in the case of $HfNCl_y$, the $dI/dV$ maps show relatively homogeneous

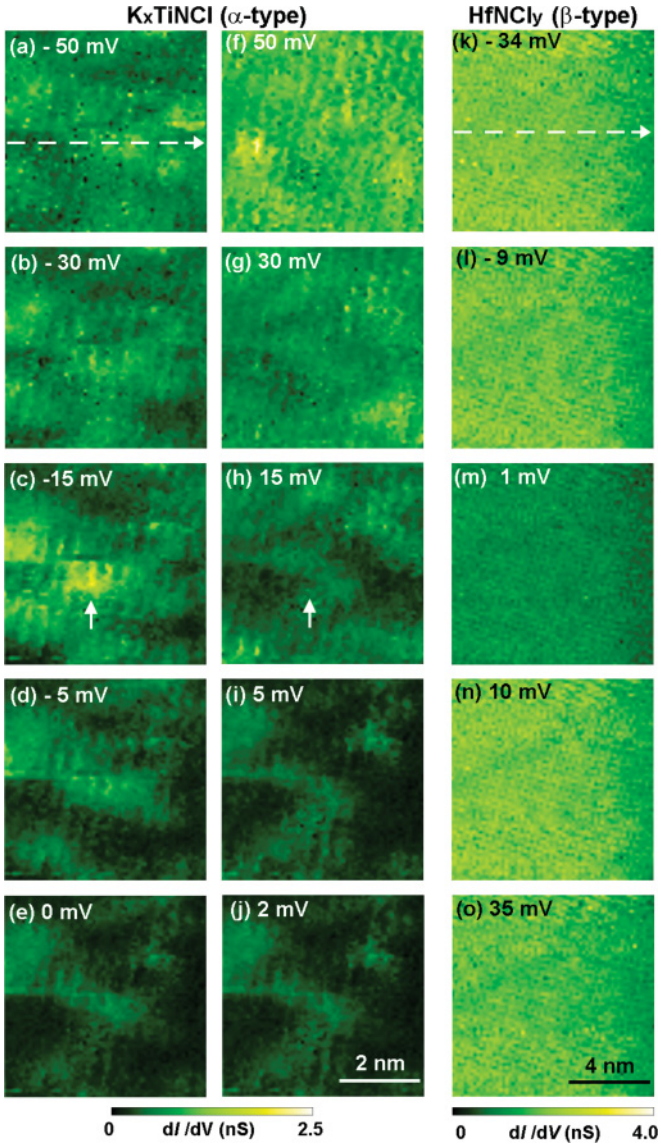


FIG. 3. (Color online) (a)–(j) The $dI/dV$ maps of $\alpha$-$K_x$TiNCl. The sample biases are (a) −50 mV, (b) −30 mV, (c) −15 mV, (d) −5 mV, (e) 0 mV, (f) 50 mV, (g) 30 mV, (h) 15 mV, (i) 5 mV, and (j) 2 mV. (k)–(o) $dI/dV$ maps on $\beta$-$HfNCl_y$ with various bias voltages of (k) −34 mV, (l) −9 mV, (m) 1 mV, (n) 10 mV, and (o) 35 mV.

distributions, which are naturally expected for the conventional BCS superconductors. This homogeneous property is noted to be in contrast to $K_x$TiNCl.

Figures 4(a) and 4(b) show the spatial variations ($x$) of $dI/dV(x,V)$ spectra measured on (a) $K_x$TiNCl [along the dashed arrow in Fig. 3(a)] and (b) $HfNCl_y$ [Fig. 3(k)]. In the case of $K_x$TiNCl [Fig. 4(a)], $dI/dV$ curves show complicated irregular shapes, but some curves show intensive peaks at negative bias (for example, $V \sim -15$ mV at the position $x = 2$–3 nm). These curves show the large spatial variations of the energy and height of peaks at negative bias side, and the $dI/dV$ magnitude at the zero bias, etc., within the scale of a few nanometers. On the contrary, in the case of $HfNCl_y$ [Fig. 4(b)], the $dI/dV$ curves show almost symmetric gap edge peaks with respect to the bias polarity, which are also

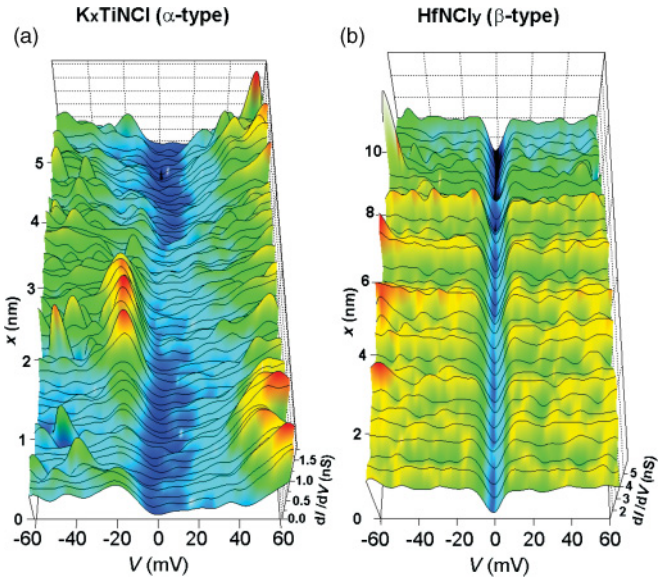


FIG. 4. (Color online) Typical spatial variation of $dI/dV$ spectrum on (a) $\alpha$-$K_x$TiNCl [along the dashed arrow in Fig. 3(a), the 5-nm displacement] and (b) $\beta$-$HfNCl_y$ [along the dashed arrow in Fig. 3(k), the 10-nm displacement].

expected for the conventional superconductors. Furthermore, the $dI/dV$ curves show spatially homogeneous electronic structures.

Figure 5(a) shows the averaged $dI/dV$ curve on $K_x$TiNCl from the observed area of Figs. 3(a)–3(j). As mentioned above, the $dI/dV$ curve shows the noticeable peak at only $V \sim -15$ mV. (The additional broad faint peak outside $V \sim -45$ mV is also observed.) However, this gap peak is broadened and the zero-bias residual conductance is relatively large. The peak voltage [shown as $\Delta_p$ in Fig. 5(a)] has been known to overestimate gap magnitude. Therefore, to obtain the suitable gap magnitude from the broadened gap structure, the fitting procedure was employed to calculate on the basis of the broadened BCS density of states proposed by Dynes *et al.*[18]

$$\frac{dI}{dV}(V) \propto \frac{d}{dV}\int_{-\infty}^{\infty}\left|\mathrm{Re}\frac{E-i\Gamma}{\sqrt{(E-i\Gamma)^2-\Delta^2}}\right| \times [f(E)-f(E+eV)]dE. \quad (1)$$

Here $f(E)$ is Fermi distribution function, $f(E) = [1 + \exp(E/k_BT)]^{-1}$. $\Gamma$, $T$, and $k_B$ are the broadening parameter, the observing temperature ($T = 4.9$ K), and Boltzmann constant, respectively. The fitting curve is presented as the dashed line in Fig. 5(a), which exhibits the best fit to the experimental curve with $\Delta \simeq 11$ meV, $\Gamma \simeq 6.2$ meV ($\Gamma/\Delta \simeq 0.6$). The fitting curves with the other possible gap symmetries such as $d$ wave and anisotropic $s$ wave were also calculated by changing the terms of $\Delta$ in Eq. (1). However, all results show no noticeable difference because of the relatively large broadening parameter $\Gamma$. Such an agreement between the BCS-based calculation and experiment is consistent with our previous BJ tunneling measurements, although the $\Gamma$ from BJ is quite small ($\Gamma/\Delta \simeq 0.1$). This may due to the pair breaking caused by the tunneling current via the STM tip depending on the surface condition. Figure 5(b) shows the spatial distribution of $\Delta$ ($\Delta$ map) on the same area of Figs. 3(a)–3(j). We have obtained only the negative-bias peak-voltage $\Delta_p$ shown by the arrow in Fig. 5(a), although it appears as a shoulder at the positive bias. Therefore, the calculated curves based on Eq. (1) were compared with the averaged $dI/dV$ curves only for the negative-bias side. The gap parameters $\Delta$ were obtained from these fittings on the several representative experimental $dI/dV$ curves averaged from those of the similar range of $\Delta_p$; then, the linear relationship of $\Delta$ and $\Delta_p$ shown in the inset of Fig. 5(a) is obtained as $\Delta$ (meV) $\simeq 0.83\Delta_p - 1.4$ ($\Delta_p > 5$ meV). According to this relationship, the $\Delta$ map was obtained from all the observed $\Delta_p$. The $\Delta$ map thus obtained is also inhomogeneous within the range of a few nanometers. This length scale is comparable or slightly shorter than that of cuprate superconductors, probably reflecting the similar electronic instability. The inset of Fig. 5(b) shows the histogram of $\Delta$. The average of $\Delta$ is $\bar{\Delta} \simeq 10.2$ meV and the standard deviation is $\sigma_\Delta \simeq 5.0$ meV. The averaged gap ratio $2\bar{\Delta}/k_BT_c$ is $\sim$15, which is almost twice as large as that of $HfNCl_y$ as mentioned later. This value is extremely larger than the standard BCS value of $\sim$3.5. It is noted that this large ratio is comparable to that of the cuprate superconductors (8–20).[12,19,20] Furthermore, the asymmetric shape of the $dI/dV$ curve and inhomogeneous gap distributions ($\sigma_\Delta \simeq 5$ meV) are also commonly seen in Bi-based cuprate superconductors.[19] The localized large gap area suggests that there exist regions where local $T_c$ would be higher than bulk $T_c$. It is noted that recent specific heat and magnetic susceptibility measurements in $Li_x$ZrNCl argued the possibility of the pairing formation mediated by spin fluctuations on the basis of the behavior of the doped insulators, which would be one of the origins of the large gap that is also one of the candidates for the pseudogap origin for cuprate superconductors.[21]

According to the band calculation of $K_x$TiNCl,[10] the pristine compound has the semiconducting gap of 1–2 eV near the Fermi energy ($E_F$). With increasing the intercalation (doping) of potassium atoms, the conduction band approaches to $E_F$, which increases the density of states at $E_F$ [$N(E_F)$]. The density of states of the conduction band is enhanced while that below the $E_F$ level still remains low against the doping. These band calculations seem to be consistent with the present STS results in $K_x$TiNCl because the slope of the tunnel spectrum curve at the positive bias side is much steeper than that at the negative bias side.

Figure 5(c) shows the averaged $dI/dV$ curve on $HfNCl_y$ from the area (10 nm $\times$ 10 nm) of Figs. 3(k)–3(o). The shape of the averaged $dI/dV$ curve is similar to the series of the $dI/dV$ curves in Fig. 4(b) because these curves were almost similar among the STS area. The $dI/dV$ curve shows bias-independent background features outside the gap voltage ($|V| = 10$–$60$ mV). These results are consistent with the band calculations,[22–24] which show that the total density of states in the vicinity of $E_F$ is almost constant within the energy region of $|E| < 0.5$ eV. The curve shows clearer gap features than that of the $K_x$TiNCl. Nevertheless, it has the finite zero-bias conductance $dI/dV$ ($V = 0$ mV). Therefore, like the case of $K_x$TiNCl, in order to obtain the suitable gap magnitude from the $dI/dV$ curve, the fitting procedures were also performed on the basis of Eq. (1). The fitting curve is shown by

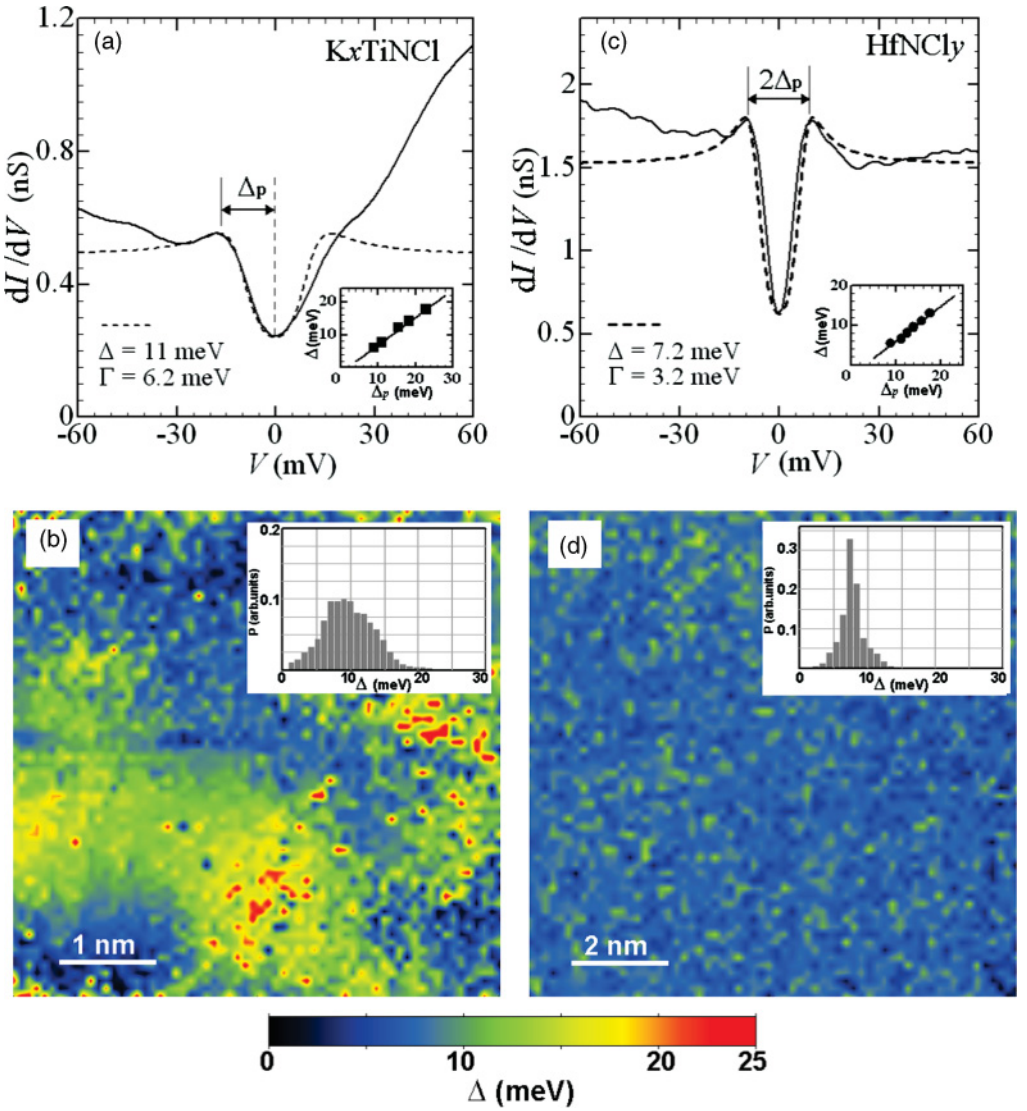


FIG. 5. (Color online) (a) Averaged $dI/dV$ curve with the fitting curves (dashed line) based on Eq. (1) and (b) $\Delta$ map on $\alpha$-$K_x$TiNCl (5 nm $\times$5 nm). (c) Averaged $dI/dV$ curve with the fitting curves (dashed line) based on Eq. (1) and (d) $\Delta$ map on $\beta$- $HfNCl_y$ (10 nm $\times$10 nm). The scale color is common with panels (b) and (d). The insets of panels (a) and (c) show the relationships between the peak gap $\Delta_p$ and the calculated gap $\Delta$ from the fitting procedures. The insets of panels (b) and (d) are the histograms of $\Delta$ maps.

dashed line in Fig. 5(c). The fitting parameter of the averaged $dI/dV$ is $\Delta = 7.2$ meV, $\Gamma = 3.2$ meV, where the ratio $\Gamma/\Delta \sim 0.44$ is similar or somewhat smaller than that of $K_x$TiNCl [Fig. 5(a)].

Figure 5(d) shows the $\Delta$ map for $HfNCl_y$. The method of the estimation of $\Delta$ was similar to that of the $K_x$TiNCl, and the peak gap magnitude $\Delta_p$ was defined as half the peak-to-peak bias voltage as shown by the arrow in Fig. 5(c). The relationship between the $\Delta_p$ and $\Delta$ is $\Delta$ (meV) $\simeq 0.88\Delta_p - 2.7$ ($\Delta_p > 5$ meV) in this $HfNCl_y$ case [shown in the inset of Fig. 5(c)]. The averaged gap $\bar{\Delta}$ and the standard deviation $\sigma_\Delta$ are $\bar{\Delta} \simeq 7.5$ meV and $\sigma_\Delta \simeq 1.9$ meV, respectively. Since the present $\sigma_\Delta$ is about 1/3 of that of $K_x$TiNCl, it is obvious that the spatial gap distribution of $HfNCl_y$ is more homogeneous than that of the $K_x$TiNCl. It is very interesting to note that the features of electronic density of states turn out to be very different between $\alpha$- and $\beta$-type compounds even though they are in the same material family. In the case of $\beta$-$HfNCl_y$, the conductance features are almost homogeneous, which is consistent with the conventional superconductors. However, the gap ratio $2\bar{\Delta}/k_B T_c \sim 7.2$ ($2\bar{\Delta} \sim 15$ meV) is about twice as large as the BCS ratio, 3.5. This large gap ratio is nearly the same as that of Bi2212 ($Bi_2Sr_2CaCu_2O_{8+\delta}$) (8–12)[12,19,20] and organic superconductors ($\sim$10).[25] It should be also noted that the gap $\bar{\Delta} \simeq 7.5$ meV is smaller than that of $K_x$TiNCl ($\bar{\Delta} \sim 10$ meV), while the $T_c$ is twice as large as that of $K_x$TiNCl. This fact indicates that the magnitude of $\Delta$ may not scale to the $T_c$ within this material family. From our recent BJ tunneling results of $HfNCl_y$, the existence of multiple gaps, $\Delta \sim 2$, 5, and 8 meV, were clarified.[26] By comparing the BJ data with the STS results, the largest gap observed in BJ turned out to correspond to the typical gap of this STS experiment. The quite large gap obtained here is too large to explain in the framework of the strong-coupling theory.[26,27] The medium gap, $\sim$5 meV,

obtained by BJ just corresponds to the recent results of heat capacity measurements,[21] while it is not observable by the STS experiment. This discrepancy may be due to the difference in the measuring methods. The BJ tunneling spectra are believed to contain information from all directions of tunneling currents detecting the unaffected surface properties. On the other hand, an STS method is sensitive to the initial surface states and detects the gap in the extremely local area. Furthermore, the strong two-dimensionality of these materials may enhance the difference in the measured properties. The complex multiple bands and Fermi surface(s) might lead to anisotropic gap such as $d$ wave or anisotropic $s$ wave. However, as mentioned above, the gap symmetries cannot be identified from the fitting procedures of the $dI/dV$ curves in both $K_x$TiNCl and $HfNCl_y$, because of the large broadenings. Further experiments must be needed to clarify these issues.

The most distinct feature in our results of two compounds is that the local density of states changes strongly within a few nanometers only in the $\alpha$ type, which is in contrast to the $\beta$ type. At present, we consider the three possible origins of the difference between $\alpha$ and $\beta$ types. The first possibility is that the inhomogeneous local density of state is due to the lattice-network specific properties. The $\alpha$-type structure has a 2D Ti-N rectangular lattice of $ab$ plane [see Fig. 1(a)], which is in a sense similar to the cuprate superconductors. This rectangular $ab$-plane network is considered to be "lower" in crystal symmetry than honeycomb network of Hf-N [see Fig. 1(b)]. Felser *et al.* predicted that the Fermi surface of electron-doped HfNCl is formed by only one band originating from Hf $5d$–N $2p$ hybridized orbital and possesses the six-fold symmetry of the Fermi surface,[24] which has higher symmetry than the rectangular network of Ti-N. On the other hand, from the band calculation of doped $K_x$TiNCl,[10] Ti $3d$–N $2p$ hybrid band mainly contributes to the Fermi surface and the shape of the two-fold symmetry of Fermi surface is assumed by the orthorhombic crystal structures. Such low dimensionality of the crystal could cause inhomogeneous electronic states because of the possible electronic fluctuations. The theoretical study of the lattice-dependent superconductivities was also reported by Kuroki *et al.*[28] It shows that the superconductivity of the honeycomb lattice is robust toward the changing of the level-offset energy between the $M$ and N networks of $M$N lattice, while that of the square lattice has the strong dependence on the level-offset energy. If we assume that these offset energies vary spatially, it is consistent with our experimental results of the more homogeneous superconductivity occurring in honeycomb lattice of $HfNCl_y$. Second, the observed inhomogeneous gap $\Delta$ in $K_x$TiNCl might be involved with the impurity states by the intercalation, because the $\Delta$ peaks occur only at the negative bias side. It is noted that the recent theoretical results[29] showed that doped isotropic semiconductors such as boron-doped diamonds would possibly become inhomogeneous (localized) superconductors induced by impurity potential. Therefore, these layered nitride superconductors, whose mother compounds are band semiconductors, are also considered to have the possibility of the impurity-induced local superconductivity. Third, these inhomogeneous features can be due to the local doping distributions by inhomogeneous intercalation. In $K_x$TiNCl, the inhomogeneous doping made by intercalated atoms could affect the local density of states and thus superconducting properties. It is noted that these results in $K_x$TiNCl are comparable to the case of Bi2212 with the strong doping dependence of the gap size.[30] On the other hand, in the case of $HfNCl_y$, the $T_c$ does not change against carrier concentration and superconducting properties are robust.[31,32] Therefore, the gap energy shows homogeneous properties even there is an inhomogeneous local doping distribution.

At last, there were still some essential ambiguities to distinguish whether the observed inhomogeneous properties were due to the bulk or the surface phenomena, because the STM-STS in principle detects the tunneling current from the surface. However, by taking the strong two dimensionality of these materials into account, the surface tunneling current of STM-STS was considered to contain the information of the bulk electronic states, as in the case of other recent STM experiments.[11–13,20] It is noted that, from the inhomogeneous $dI/dV$ spectra and relatively large gap-broadening parameter $\Gamma$, especially in $K_x$TiNCl, the possibility of the initial contamination that affects the strongly disordered electronic states cannot be excluded. More detailed kinds of experiments must be needed with higher purity compounds as well as other layered nitride compounds to elucidate the essential relationship between the lattice symmetry and the electronic structure in the superconducting states.

## IV. SUMMARY

We have carried out the STM-STS measurements of both $\alpha$-$K_x$TiNCl and $\beta$-$HfNCl_y$ superconductors. From the STM images, the clear atomic structures of the rectangular lattice on $\alpha$-$K_x$TiNCl and the triangular lattice on $\beta$-$HfNCl_y$ were confirmed. The $dI/dV$ spectra show qualitatively different features between these superconductors; the spatial distribution of the tunneling spectrum and the gap magnitude on $\alpha$-$K_x$TiNCl are inhomogeneous, while those on $\beta$-$HfNCl_y$ show relatively homogeneous distribution. The averaged gap magnitudes of $\bar{\Delta} \simeq 10.2$ meV (the standard deviation of gap $\sigma_\Delta \simeq 5.0$ meV) and $\bar{\Delta} \simeq 7.5$ meV ($\sigma_\Delta \simeq 1.9$ meV) for $\alpha$-$K_x$TiNCl and $\beta$-$HfNCl_y$, with the gap ratios $2\Delta/k_BT_c \simeq 15$ and 7.2, respectively, are extremely large as compared with BCS theory. The difference in the gap ratio between them is considered to be caused by the lattice symmetry difference itself or induced by the difference in the local doping and impurity distributions in these chemically reactive compounds.

## ACKNOWLEDGMENTS

We thank the Natural Science Center for Basic Research and Development, Hiroshima University, for supplying liquid helium. This work has been supported by the Japan Society for the Promotion of Science (JSPS) through its "Funding Program for World-Leading Innovative R&D on Science and Technology (FIRST) Program" and by Grants-in-Aid for Young Scientist (Start-up No. 18810021) and Scientific Research (No. 19105006, No. 19051011, No. 19014016, and No. 19540370) of the Ministry of Education, Culture, Sports, Science, and Technology (MEXT) of Japan.

[1] S. Yamanaka, K. Hotehana, and H. Kamiji, Nature (London) **392**, 580 (1998).
[2] J. Nagamatsu, N. Nakagawa, T. Muraoka, Y. Zenitani, and J. Akimitsu, Nature (London) **410**, 63 (2001).
[3] Y. Kamihara, T. Watanabe, M. Hirano, and H. Hosono, J. Am. Chem. Soc. **130**, 3296 (2008).
[4] Y. Taguchi, T. Kawabata, T. Takano, A. Kitora, K. Kato, M. Takata, and Y. Iwasa, Phys. Rev. B **76**, 064508 (2007).
[5] H. Tou, Y. Maniwa, and S. Yamanaka, Phys. Rev. B **67**, 100509(R) (2003).
[6] T. Ekino, T. Takasaki, T. Muranaka, H. Fujii, J. Akimitsu, and S. Yamanaka, Phys. B (Amsterdam, Neth.) **328**, 23 (2003).
[7] T. Takasaki, T. Ekino, H. Fujii, and S. Yamanaka, J. Phys. Soc. Jpn. **74**, 2586 (2005).
[8] T. Takasaki, T. Ekino, and S. Yamanaka, Phys. C (Amsterdam, Neth.) **445-448**, 77 (2006).
[9] Y. Taguchi, M. Hisakabe, and Y. Iwasa, Phys. Rev. Lett. **94**, 217002 (2005).
[10] S. Yamanaka, T. Yasunaga, K. Yamaguchi, and M. Tagawa, J. Mater. Chem. **19**, 2573 (2009).
[11] K. M. Lang, Y. Madhavan, J. E. Hoffman, E. W. Hudson, H. Eisaki, S. Uchida, and J. C. Davis, Nature (London) **415**, 412 (2002).
[12] Ø. Fischer, M. Kugler, I. Maggio-Aprile, C. Berthod, and Ch. Renner, Rev. Mod. Phys. **79**, 353 (2007).
[13] T. Hanaguri, C. Lupien, Y. Kohsaka, D-H. Lee, M. Azuma, M. Takano, H. Takagi, and J. C. Davis, Nature (London) **430**, 1001 (2004).
[14] L. Zhu and S. Yamanaka, Chem. Mater. **15**, 1897 (2003).
[15] T. Ekino, T. Takasaki, R. A. Ribeiro, T. Muranaka, and J. Akimitsu, J. Phys.: Conf. Ser. **61**, 278 (2007).
[16] A. Sugimoto, T. Ekino, and H. Eisaki, J. Phys. Soc. Jpn. **77**, 043705 (2008).
[17] A. Sugimoto, K. Shohara, T. Ekino, and S. Yamanaka, J. Phys.: Conf. Ser. **150**, 052251 (2009).
[18] R. C. Dynes, V. Narayanamurti, and J. P. Garno, Phys. Rev. Lett. **41**, 1509 (1978).
[19] A. Sugimoto, S. Kashiwaya, H. Eisaki, H. Kashiwaya, H. Tsuchiura, Y. Tanaka, K. Fujita, and S. Uchida, Phys. Rev. B **74**, 094503 (2006).
[20] K. McElroy, J. Lee, J. A. Slezak, D. H. Lee, H. Eisaki, S. Uchida, and J. C. Davis, Science **309**, 1048 (2005).
[21] Y. Kasahara, T. Kishiume, T. Takano, K. Kobayashi, E. Matsuoka, H. Onodera, K. Kuroki, Y. Taguchi, and Y. Iwasa, Phys. Rev. Lett. **103**, 077004 (2009).
[22] P. M. Woodward and T. Vogt, J. Solid State Chem. **138**, 207 (1998).
[23] I. Hase and Y. Nishihara, Phys. Rev. B **60**, 1573 (1999).
[24] C. Felser and R. Seshadri, J. Mater. Chem. **9**, 459 (1999).
[25] T. Arai, K. Ichimura, K. Nomura, S. Takasaki, J. Yamada, S. Nakatsuji, and H. Anzai, Phys. Rev. B **63**, 104518 (2001).
[26] T. Takasaki, T. Ekino, A. Sugimoto, K. Shohara, S. Yamanaka, and A. M. Gabovich, Eur. Phys. J. B **73**, 471 (2010).
[27] F. Marsiglio and J. P. Carbotte, Phys. Rev. B **33**, 6141 (1986).
[28] K. Kuroki, Sci. Technol. Adv. Mater. **9**, 044202 (2008).
[29] Y. Yanase and N. Yorozu, J. Phys. Soc. Jpn. **78**, 034715 (2009).
[30] N. Miyakawa, J. F. Zasadzinski, L. Ozyuzer, P. Guptasarma, D. G. Hinks, C. Kendziora, and K. E. Gray, Phys. Rev. Lett. **83**, 1018 (1999).
[31] Y. Taguchi, A. Kitora, and Y. Iwasa, Phys. Rev. Lett. **97**, 107001 (2006).
[32] T. Takano, T. Kishiume, Y. Taguchi, and Y. Iwasa, Phys. Rev. Lett. **100**, 247005 (2008).